Journal of Alloys and Compounds 512 (2012) 340–350

Contents lists available at SciVerse ScienceDirect

Journal of Alloys and Compounds

journal homepage: www.elsevier.com/locate/jallcom

Microstructural evolution in damaged IN738LC alloy during various steps of rejuvenation heat treatments

Sayyed Shahabeddin Hosseini*, Said Nategh, Ali-Akbar Ekrami

Department of Materials Science and Engineering, Sharif University of Technology, P.O. Box 11155-9466, Azadi Ave., Tehran, Iran

ARTICLE INFO

Article history:
Received 4 June 2011
Received in revised form
26 September 2011
Accepted 29 September 2011
Available online 8 October 2011

Keywords:
Nickel base superalloy
Rejuvenation heat treatment
Microstructure

ABSTRACT

IN738LC is one of the superior nickel base superalloys utilized at high temperatures in aggressive environments. However, experiencing high temperatures and stresses during service causes microstructure deterioration and degradation of mechanical properties in this alloy. To restore the microstructure and mechanical properties of the degraded alloy, rejuvenation heat treatments can be considered. In this study, the evolution of microstructural features in a creep damaged IN738LC superalloy during different stages of rejuvenation heat treatment cycles was investigated. During solution treatment stage, dissolution of coarsened γ′ precipitates, grain boundary films and transition zone around primary MC carbides took place. Solution treatment at high temperature led to lower volume fraction and smaller size of remnant γ′ precipitates and further dissolution of grain boundary films and caused MC carbides to be remained without the surrounding transition zone. In addition, fine γ′ precipitates formed during the subsequent cooling, namely cooling precipitates, were detected in higher contents after solutionizing at higher temperatures. It was found that slower cooling rates after solution treatment gave rise to coarser γ′ precipitates with higher volume fraction. Among all heat treatment cycles investigated, double solution treatment at 1190 °C/4 h/FC (furnace cooling) + 1120 °C/2 h/AC (air cooling) followed by aging at 845 °C/24 h/AC was successful to revert the microstructure back to its virgin state.

1. Introduction

Nickel base superalloys are widely used in a variety of applications, at high temperatures and stresses, in aggressive atmospheres [1,2]. The unique properties required in these alloys can be attributed to an FCC nickel base solid solution matrix which is strengthened by solutes and precipitates. The precipitates in these alloys are principally the Ni_3(Al,Ti,Nb)-type intermetallic compound and carbides, with proper structure, size, shape, and distribution [3]. Extensive studies have shown that prolonged thermal and stress exposure during service causes various microstructural damage in these alloys, all of which have detrimental effect on mechanical properties, such as tensile strength and creep resistance [4–8]. However, restoration of microstructure and mechanical properties to levels equivalent to the original material has been achieved by the use of proper refurbishment procedures. Thus, implementation of appropriate refurbishment processes has the potential to significantly extend the useful life of degraded components. Moreover, since material deterioration necessitates the replacement of components, the high cost of new replacement parts has provided a strong incentive for developing proper refurbishment procedures as economic methods of extending service lives of damaged parts [9,10].

Thermal processing, including rejuvenation heat treatment alone or recovery cycles incorporating both rejuvenation heat treatment and hot isostatic pressing (HIPping), is a critical step in refurbishment of degraded components. Rejuvenation heat treatments, consisting of two main stages of solution and aging treatments, are targeted at achieving maximum re-establishment of the original microstructure and initial properties. Improper heat treatment, however, may have deleterious effects, such as formation of undesirable phases, incipient melting, crack initiation, and oxidation during service. The influence of rejuvenation heat treatments on recovery of mechanical properties in damaged nickel base superalloys has been studied by numerous authors. They correlated the observed recovery to microstructural restoration (through re-solution and re-precipitation), sintering of cavities (by vacancy diffusion under the action of surface tension and/or supplied pressure), inhibition of growth in grain boundary cavities (*via* isolating them within the grain interiors through recrystallization or grain growth), and changes in dislocations structure [11–20].

Superalloy IN738LC is one of the most widely used nickel base superalloys utilized to manufacture hot section components. It is well known that IN738LC has a multiphase microstructure and owns its high temperature strength from the fine particles of Ll_2 type ordered γ′ [Ni_3(Al,Ti)] phase coherently precipitated in the

* Corresponding author. Tel.: +98 912 5673052; fax: +98 21 66005717.
E-mail address: shahabeddinhosseini@gmail.com (S.S. Hosseini).

0925-8388/$ – see front matter © 2011 Elsevier B.V. All rights reserved.
doi:10.1016/j.jallcom.2011.09.094

Table 1
Chemical composition of the as-received IN738LC.

Element	Ni	Cr	Mo	Al	Ti	Ta	W	Co	Nb	Zr	C
Wt%	Balance	16.3	1.65	3.2	3.22	1.8	2.7	8.5	0.7	0.03	0.1

(FCC) γ matrix. The effect of rejuvenation heat treatments on microstructure and mechanical properties of damaged IN738LC superalloy has been investigated by several researchers [21–25]. They explored the possibility of restoring the microstructure and mechanical properties of degraded IN738LC superalloy. However, there is not much published information on microstructural evolution in degraded IN738LC superalloy during different stages (*i.e.* solution and aging treatments) of rejuvenation heat treatment cycles in details.

This investigation concerns the microstructural aspects of the IN738LC alloy. The virgin alloy was initially damaged by interrupted creep test and then rejuvenation heat treatment cycles were performed on the damaged alloy. It is the goal of the present study to have a deep insight into the changes of microstructural features in the damaged IN738LC superalloy during different steps of rejuvenation heat treatment cycles.

2. Experimental procedure

The experiments were performed on polycrystalline IN738LC nickel base superalloy. The chemical composition of the alloy, determined by XRF analysis, is given in Table 1. Cylindrical bars, 10 mm in diameter and 95 mm in length, were produced under vacuum atmosphere by investment casting. The cast bars then underwent two successive heat treatments under argon atmosphere: Homogenization and standard heat treatment. Homogenization or full solution heat treatment consisted of solution treatment at 1190 °C for 4 h and subsequent furnace cooling to room temperature. Standard heat treatment consisted of solution treatment at 1120 °C for 2 h and subsequent air cooling to room temperature (partial solution) and aging treatment at 845 °C for 24 h and, finally, air cooling to room temperature.

In order to damage the alloy, creep tests were performed at 926 °C under stress of 170 MPa, according to ASTM E139, on round test samples with gauge length of 20 mm and diameter of 4 mm and interrupted after 200 h from the beginning of the tests. Samples temperature was controlled within ±2 °C by attached thermocouples. The interrupted creep test conditions were chosen based on the creep–rupture curves given in Ref. [26] to damage the alloy within a reasonable time. The damaged alloy was then subjected to different rejuvenation heat treatments under argon atmosphere with the aim of restoring the degraded microstructure and investigating the microstructure evolution during different stages of rejuvenation heat treatment cycles. The different heat treatment schedules are given in Table 2.

Samples preparation for metallographic examination was carried out by sectioning, grinding, electropolishing with a solution of 45% acetic acid, 45% butanol and 10% perchloric acid at 20–25 V for 25 s and, finally, electroetching with the same solution at 4–5 V for 3–4 s. The microstructures were examined using a Philips XL-40 scanning electron microscope (SEM). Measurement of the γ′ particles characteristics was conducted on the SEM micrographs using Image Tool software, a semi-quantitative image analyser. Since the quantitative metallograghic investigation is principally a statistical measurement, many images from different conditions were analysed. However, only one of each is shown in the present study as being representative. Some features of the γ′ precipitate particles were determined, such as volume fraction, Feret diameter, aspect ratio and roundness. Feret diameter is defined as the diameter of a circle with an equal area of a feature of arbitrary shape. As the precipitates morphology changed during the interrupted creep test and different rejuvenation heat treatments, Feret diameter was chosen as a measure of particle size to compare particle sizes with different morphologies. Aspect ratio and roundness were also measured to quantify and compare the morphologies of γ′ particles in different conditions. Aspect ratio is the ratio of the largest side to the smallest side of a particle. Roundness is a measure of the particle's spheroidal morphology. More deviation from spheroidal morphology less roundness value is measured and a circle and a cube have roundness values of 1 and 0.75, respectively.

3. Results and discussion

3.1. Virgin alloy

Fig. 1 represents microstructure of the as-cast IN738LC after homogenization and standard heat treatment. The microstructure is typical for a virgin cast and heat treated nickel base superalloy: a bimodal morphology of intragranular strengthening γ′ precipitates, consisting of primary cuboidal γ′ particles with an average edge size of 720 nm and secondary spheroidal γ′ precipitates with an average diameter of 90 nm; coarse erratic grain boundary γ′ precipitates; massive irregularly shaped discrete primary MC carbides dispersed both at the grain boundaries and in the grain interiors during solidification; and fine secondary $M_{23}C_6$ carbides primarily precipitated along the grain boundaries. This reasonable distribution of microstructural features guarantees the excellent mechanical properties of the alloy. The cast IN738LC superalloy after homogenization and standard heat treatment, containing such microstructural constituents, is considered as *virgin alloy* in the current study.

3.2. Degradation of virgin alloy

The virgin alloy was degraded by interrupted creep test at 926 °C and 170 MPa for 200 h. The creep curve obtained for the virgin alloy at 926 °C and 170 MPa is represented in Fig. 2(a). Virgin alloy sample had 317.4 h creep life and showed 9.2% creep strain at rupture. Fig. 2(b) displays the creep curve for the virgin alloy gained after interrupted creep test. Point (P) on the curve indicates the point at which the creep test was interrupted. It can be noted that the creep strain at interrupted point was 3.1%. Considering the curves in Fig. 2, it can be found that the test was interrupted at tertiary creep.

The microstructures of the virgin alloy before and after interrupted creep test were compared to demonstrate the degree of microstructural deterioration (see Figs. 1 and 3). Fig. 3 shows SEM micrographs of the virgin alloy after interrupted creep test. As can be observed, interrupted creep test resulted in significant changes in microstructure. It is evident from Fig. 3(a) that coarsening of both primary and secondary γ′ precipitates has occurred. In

Table 2
Rejuvenation heat treatment schedules for the creep damaged IN738LC.

Cycle	Full solution			Partial solution			Aging		
	Temperature (°C)	Time (h)	Cooling rate	Temperature (°C)	Time (h)	Cooling rate	Temperature (°C)	Time (h)	Cooling rate
A	–	–	–	1120	2	AC	–	–	–
B	–	–	–	1160	2	AC	–	–	–
C	1190	2	AC	–	–	–	–	–	–
D	1190	4	AC	–	–	–	–	–	–
E	–	–	–	1120	2	SC	–	–	–
F	1190	4	FC	–	–	–	–	–	–
G	1190	4	FC	1120	2	AC	–	–	–
H[a]	–	–	–	1120	2	AC	845	24	AC
I	1190	4	FC	1120	2	AC	845	24	AC
J	–	–	–	1160	2	AC	845	24	AC

AC: air cooling, FC: furnace cooling, SC: slow cooling (20 °C/min).
[a] Standard heat treatment cycle for IN738LC.

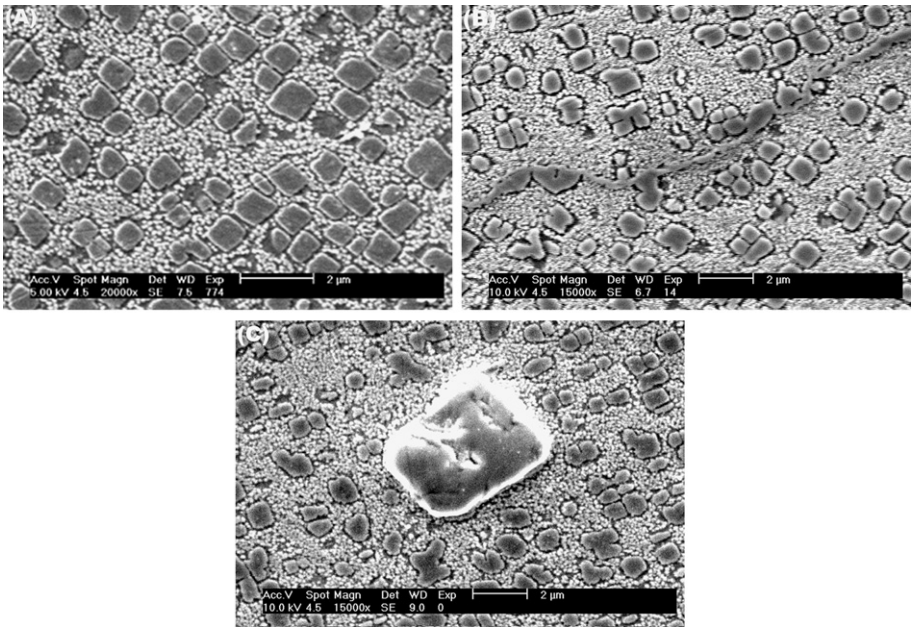

Fig. 1. SEM micrographs of virgin alloy showing: (A) intragranular bimodal γ′ precipitates; (B) grain boundary region; and (C) primary MC carbide.

particular, the large cuboidal primary γ′ precipitates coarsened at the expense of the fine secondary ones and converted into oval-shaped or spheroidal type. These led to a decrease in the density of secondary particles and an increase in the inter-particle spacing. The coarsening of γ′ precipitates in nickel base alloys is believed to be in accordance with LSW theory and subsequent modifications and driven by the reduction in total interfacial energy. The changes in γ′ precipitates characteristics are also confirmed by the data for the virgin and damaged alloys in Table 3. Table 3 summarizes the data from statistical measurement of γ′ precipitates characteristics at different conditions. The virgin alloy after interrupted creep test is considered as *damaged alloy* in the present investigation. Furthermore, as is comparatively seen in Figs. 1(b) and 3(b), during the interrupted creep test, continuous films of γ′ phase formed along the grain boundaries. The γ′ precipitates in grain boundary regions appear to have coarsened and merged with each other and, consequently, resulted in the formation of grain boundary films that envelop the grain boundaries. However, no evidence of continuous networks of secondary $M_{23}C_6$ carbides on grain boundaries was observed in the damaged microstructure.

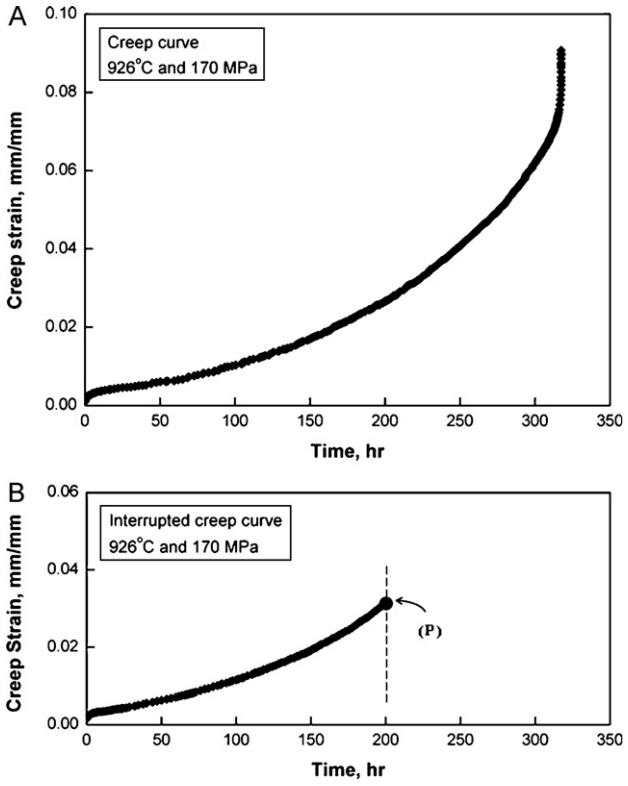

Fig. 2. (A) Creep curve for virgin alloy at 926 °C under stress of 170 MPa and (B) creep curve for virgin alloy obtained after interrupted creep test at 926 °C and 170 MPa for 200 h. Point (P) indicates the interrupted point on the creep curve.

Primary MC carbides are other microstructural features apparent in the damaged alloy. Fig. 3(c) shows the microstructure of the damaged alloy emphasizing the primary MC carbide precipitates. Comparison of the MC carbides in the virgin alloy (Fig. 1(c)) with those in the damaged alloy (Fig. 3(c)) reveals that, during the interrupted creep test, discrete primary MC carbides were surrounded by a continuous film which seems to be a transition zone that was formed due to the occurrence of primary MC carbides decomposition. According to Lvov et al. [27], during thermal exposure, the primary MC carbides with high carbon content serve as a carbon resource and γ matrix as a Ni, Cr, and Co reservoir. Outward diffusion of carbon from the primary MC carbides into the surrounding matrix and inward diffusion of Ni, Cr, and Co from the γ matrix into the primary MC carbides in the opposite direction develop a transition zone between the primary MC carbides and their perimeter. However, the short-term interrupted creep test, performed in the present study, could not create the condition favorable for the formation of lower-order $M_{23}C_6$ carbides and other probable primary MC decomposition products in the transition zone. This is presumably why no evidence of $M_{23}C_6$ carbides and other possible MC carbide decomposition products was observed.

Additionally, consistent with the results of Jianting et al. [28], microstructural examination of damaged alloy showed that no

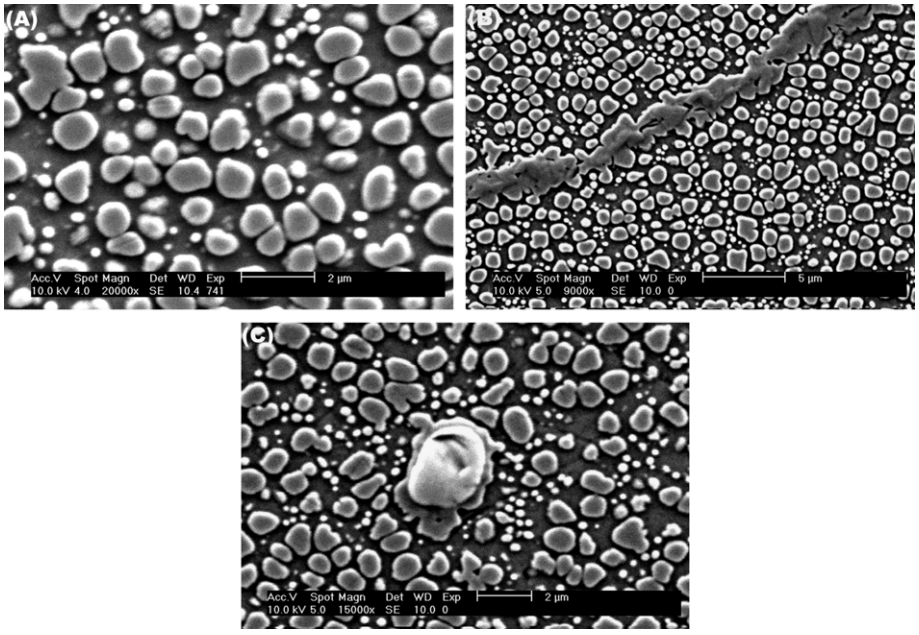

Fig. 3. SEM micrographs of damaged alloy showing: (A) intragranular coarsened γ′ precipitates; (B) continuous grain boundary film; and (C) primary MC carbide surrounded by transition zone.

voids and cracks were found along the grain boundaries. Cavity nucleation is generally believed to commence at an early stage of creep deformation and continue during the creep life [22,29]. Thus, a number of cavities might be present in the damaged alloy that are too small to be detected *via* metallographic examination. Such minute cavities can be mainly eliminated by the application of hot isostatic pressing.

3.3. Microstructural changes during rejuvenation heat treatment

3.3.1. Solution treatment and subsequent cooling

Solution treatment temperatures were chosen at three different temperatures (1120, 1160 and 1190 °C) to examine the influence of solutionizing temperature on microstructure of the damaged alloy. The micrographs from the damaged microstructure after solution

Table 3
Data from statistical measurement of γ′ precipitates characteristics in virgin and creep damaged alloy and damaged alloy after rejuvenation heat treatment cycles A to J.

Condition	Type of precipitates	Volume fraction	Feret diameter (nm)	Aspect ratio	Roundness
Virgin alloy	Primary	0.28	847.15	1.45	0.71
	Secondary	0.21	91.34	1.12	1.00
Damaged alloy	Primary	0.37	1328.3	1.36	0.87
	Secondary	0.10	163.75	1.17	1.00
Cycle A[a]	Remnant	0.19	815.66	1.28	0.93
	Cooling	–	–	–	–
Cycle B	Remnant	0.13	410.44	1.31	0.89
	Cooling	0.32	86.17	1.11	1.00
Cycle C[b]	Remnant	–	–	–	–
	Cooling				
Cycle D[b]	Remnant	–	–	–	–
	Cooling				
Cycle E	Remnant	0.22	957.81	1.26	0.91
	Cooling	0.26	291.25	1.32	0.82
Cycle F[c]	Remnant	–	–	–	–
	Cooling	0.48	802.32	1.47	0.69
Cycle G[a]	Remnant	0.20	776.94	1.44	0.70
	Cooling	–	–	–	–
Cycle H	Remnant	0.21	862.78	1.25	0.95
	Cooling	0.26	88.47	1.12	1.00
Cycle I	Primary	0.27	845.67	1.43	0.72
	Secondary	0.22	94.12	1.11	1.00
Cycle J	Remnant	0.15	412.18	1.29	0.90
	Cooling	0.33	92.15	1.12	1.00

[a] Cooling precipitates are too fine to be detected.
[b] Remnant and cooling precipitates are too fine to be distinguished from each other.
[c] Remnant precipitates are too fine to be detected.

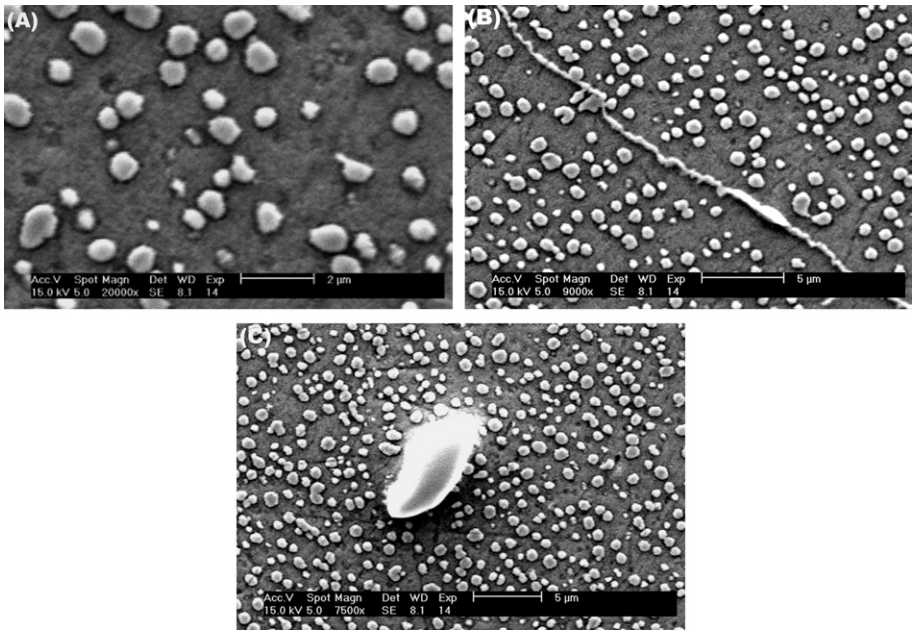

Fig. 4. Microstructure of damaged alloy after cycle A: (A) remnant γ′ precipitates within grain interiors; (B) continuous film on grain boundary region; and (C) primary MC carbide.

treatments at different temperatures and subsequent air cooling to room temperature (heat treatment cycles A to D) are shown in Figs. 4–7. The measured Feret diameter and volume fraction for γ′ precipitates in the damaged alloy before and after cycle A (Table 3) and comparison of Figs. 3(a) and 4(a) implies that 1120 °C/2 h/AC solution treatment (cycle A) gave rise to a decrease in the size and volume fraction of coarsened γ′ precipitates and produced a nearly unimodal–spheroidal γ′ microstructure. This indicates that as the solution treatment temperature in cycle A (1120 °C) is a subsolvus temperature for γ′ dissolution in IN738LC, partial dissolution of coarsened γ′ precipitates in the damaged alloy has occurred and a large number of undissolved particles, namely *remnant precipitates*, were remained within the matrix (Fig. 4(a)).

The microstructural examination revealed that, apart from γ′ precipitates, continuous grain boundary films were also affected by cycle A. Fig. 4(b) displays a segment of the continuous films observed along the grain boundaries in the damaged alloy after cycle A. Measurement of thickness of the grain boundary films in the damaged alloy and that after cycle A implies that the thickness of the grain boundary films after cycle A is less than that in the damaged alloy. This suggests that, during the solution treatment at 1120 °C/2 h, the continuous grain boundary films were dissolved partially.

The influence of 1120 °C/2 h/AC solution treatment (cycle A) on the MC carbides is also noticeable. Fig. 4(c) shows a blocky MC carbide in the microstructure after cycle A. Comparing the MC

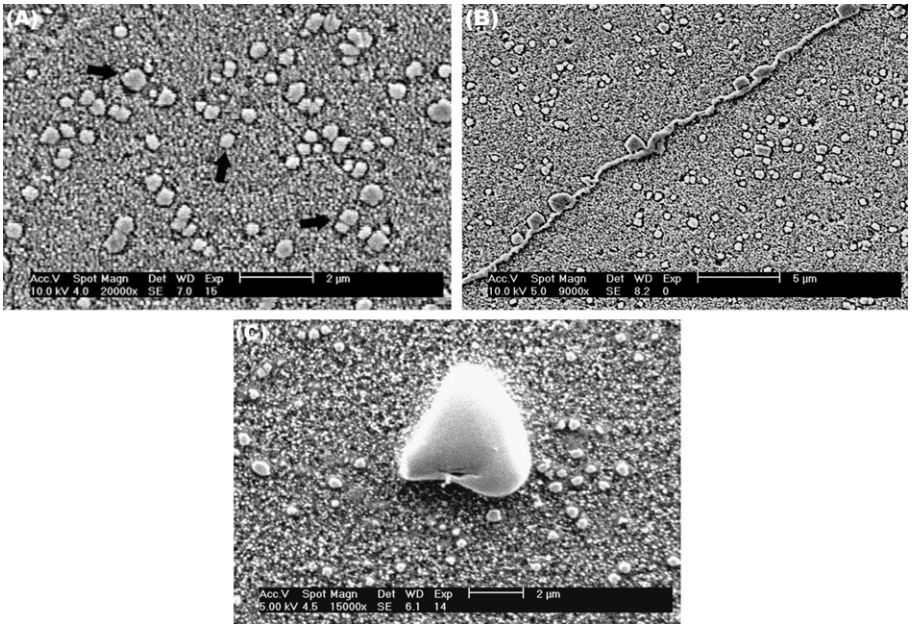

Fig. 5. SEM micrographs of damaged alloy after cycle B showing: (A) intragranular duplex size γ′ precipitates. Arrows indicate remnant precipitates; (B) continuous film on grain boundary area; and (C) primary MC carbide.

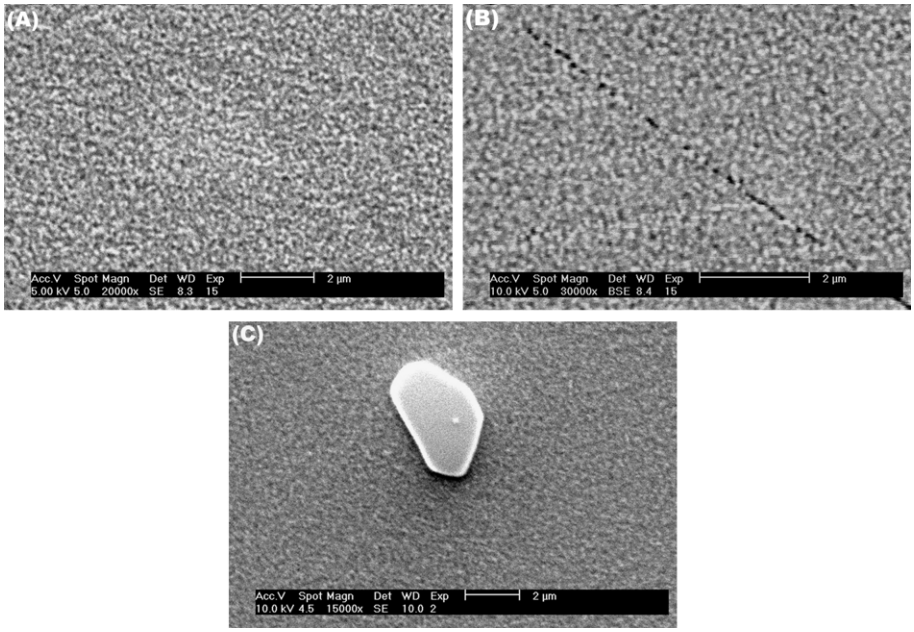

Fig. 6. SEM micrographs of damaged alloy after cycle C showing: (A) fine γ′ precipitates within grains; (B) grain boundary region; and (C) primary MC carbide.

carbides before and after cycle A (Figs. 3(c) and 4(c)), it can be seen that 1120 °C/2 h/AC solution treatment has eliminated the transition zone formed around the MC carbides during the interrupted creep test and left undecomposed MC carbides undissolved. In fact, despite the partial dissolution of γ′ precipitates in the grain interiors and continuous films on the grain boundaries, entire dissolution of the transition zone seems to have taken place. In light of these findings, it can be deduced that the solution treatment temperature in cycle A (1120 °C) lies above the transition zone solvus temperature.

The SEM studies revealed that, due to the increased solubility of γ′ forming elements in γ matrix, solution treatment at higher temperature led to further dissolution of coarsened γ′ precipitates and, consequently, finer widely spaced remnant precipitates with lower volume fraction were remained. This can be readily found by considering Figs. 4(a) and 5(a) and the data from statistical measurement of Feret diameter and volume fraction for remnant precipitates in the damaged microstructure after heat treatment cycles A and B (Table 3). Fig. 5(a) shows the γ′ microstructure after 1160 °C/2 h/AC solution treatment (cycle B). As can be observed, cycle B yielded a duplex-size unimodal precipitate microstructure, in which many fine secondary γ′ precipitates can be found adjacent to remnant ones. It is to be noted that further dissolution of remnant precipitates incorporates more solute atoms into the γ matrix, leading to the formation of fine secondary precipitates, namely *cooling precipitates*, in the space between the remnant ones due to solute ejection from the matrix during subsequent air cooling to room temperature. Indeed, the appearance of fine cooling precipitates

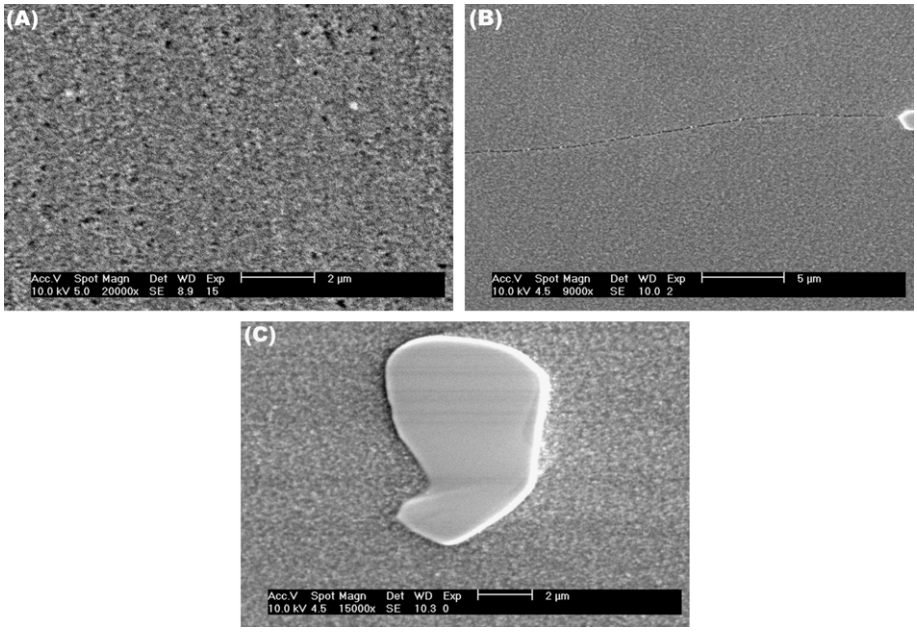

Fig. 7. Microstructure of damaged alloy after cycle D: (A) very fine γ′ precipitates within grain interiors; (B) grain boundary region; and (C) primary MC carbide.

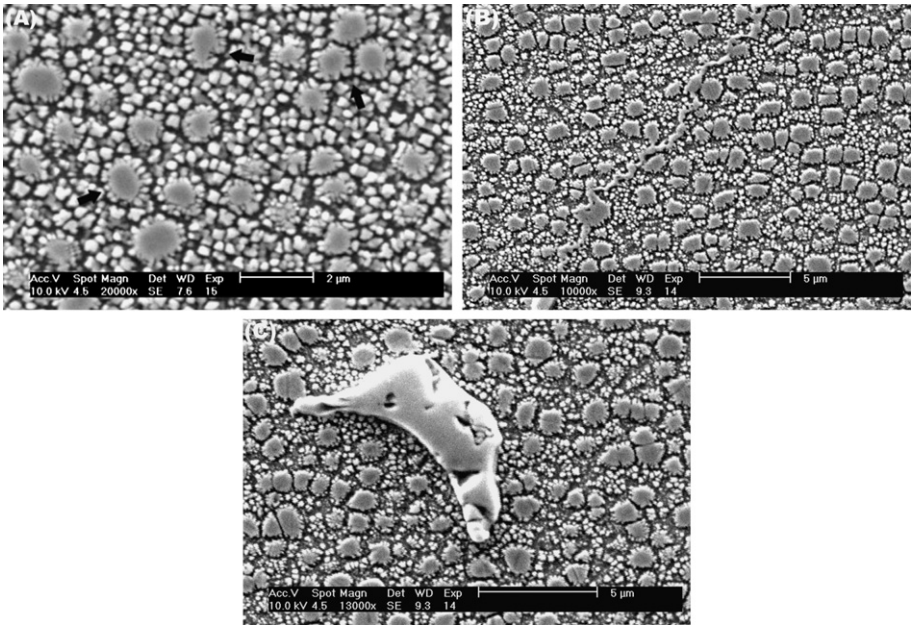

Fig. 8. Microstructure of damaged alloy after cycle E: (A) intragranular duplex size γ′ precipitates. Arrows indicate remnant precipitates agglomerated with neighboring cooling ones; (B) continuous film on grain boundary area; and (C) primary MC carbide.

compensates for the decrease in volume fraction of the coarse remnant ones. Such fine cooling precipitates can be observed in Fig. 5(a). The aspect ratio and roundness values measured for these cooling precipitates (Table 3) indicate near spherical morphology. In addition, as seen in Fig. 5, the grain boundaries are covered with continuous films and, as was the case for the microstructure after cycle A, partial dissolution of grain boundary films and disappearance of transition zone around MC carbides have occurred after cycle B (compare Figs. 3(b) and (c) with 5(b) and (c), respectively).

Fig. 6 exhibits the microstructure after 1190 °C/2 h/AC solution treatment (cycle C). It appears that most of coarsened γ′ precipitates in the damaged alloy were dissolved in the matrix and only fine remnant precipitates have remained in proximity to the fine cooling ones (Fig. 6(a)). Moreover, compared to the microstructure obtained after cycle B (Fig. 5(a)), it seems that further dissolution of remnant precipitates at higher solutionizing temperature (1190 °C) was accompanied by further formation of fine cooling ones, and dimensional difference between the remnant and cooling precipitates became less appreciable. This causes the uniform distribution of fine γ′ precipitates in the microstructure after cycle C. It is also important to note that longer solution treatment at 1190 °C produces even finer precipitates, as can be seen in Fig. 7(a). Fig. 7(a) shows the γ′ microstructure after 1190 °C/4 h/AC solution treatment (cycle D). In this condition, one might think of complete dissolution of remnant precipitates during the 1190 °C/4 h solution treatment. However, since solution treatment at 1235 °C for at least 4 h has been reported to be required for entire dissolution of γ′ phase in IN738LC alloy [30], it can be inferred that complete dissolution of remnant precipitates could not occur after cycle D and there might still exist very fine remnant precipitates that are too fine to be distinguished from the adjacent fine cooling ones.

The effect of high temperature solution treatment on the grain boundary films is another aspect which should be taken into account. Figs. 6(b) and 7(b) show the grain boundary areas in the damaged alloy after cycles C and D, respectively. As it is evident, no grain boundary film is observed along the grain boundaries. It seems that the grain boundaries were depleted from continuous films extensively and only very fine discrete precipitates can be observed in these regions. This suggests that nearly complete dissolution of grain boundary films has happened. Moreover, since the primary MC carbides have been reported to precipitate during the solidification process, even high temperature solution treatments (cycles C and D) were not able to dissolve the undecomposed primary MC carbides and, resultantly, the MC carbides free from the surrounding transition zone were observed in many locations (see Figs. 6(c) and 7(c)).

Cooling rate after solution treatment is also an impressive parameter on the damaged microstructure. Cycles E and F were designed to investigate the effect of cooling rate. Fig. 8 represents the microstructure produced after cycle E, in which cooling was performed subsequent to the 1120 °C/2 h solution treatment with the rate of 20 °C/min. Comparing the γ′ microstructures obtained after cycles A and E (Figs. 4(a) and 8(a), respectively), it can be readily found that, in contrast with the single size unimodal γ′ microstructure without cooling precipitates formed after cycle A, a duplex size unimodal γ′ microstructure with relatively large cooling precipitates was gained. Additionally, according to the statistical parameters for γ′ precipitates after cycles A and E (Table 3), higher volume fraction of γ′ precipitates was obtained after cycle E. The coarser precipitates in Fig. 8(a) are remnant precipitates which formed after 1120 °C/2 h solution treatment and the finer ones are cooling precipitates which formed during the slow cooling (20 °C/min). The formation of coarse remnant and cooling precipitates after cycle E might be correlated with the fact that solute ejection from the matrix solid solution continues during the slower cooling [30], leading to the formation and growth of relatively large cooling precipitates and some growth of remnant ones. Furthermore, as seen in Fig. 8(a), merging of remnant precipitates with neighboring cooling ones has occurred. Such an agglomeration of coarse and fine precipitates has been reported by some investigators and presented as a precipitate growth mechanism [30–32]. Contrarily, the lack of cooling precipitates in the damaged microstructure after cycle A (Fig. 4(a)) can be related to the high cooling rate during the air cooling from 1120 °C to room temperature. While air cooling, the nucleation rate of cooling precipitates is expected to be high, resulting in the formation of finer cooling precipitates. Therefore, there might be very fine cooling precipitates that are too fine to be detected within the limits of the used

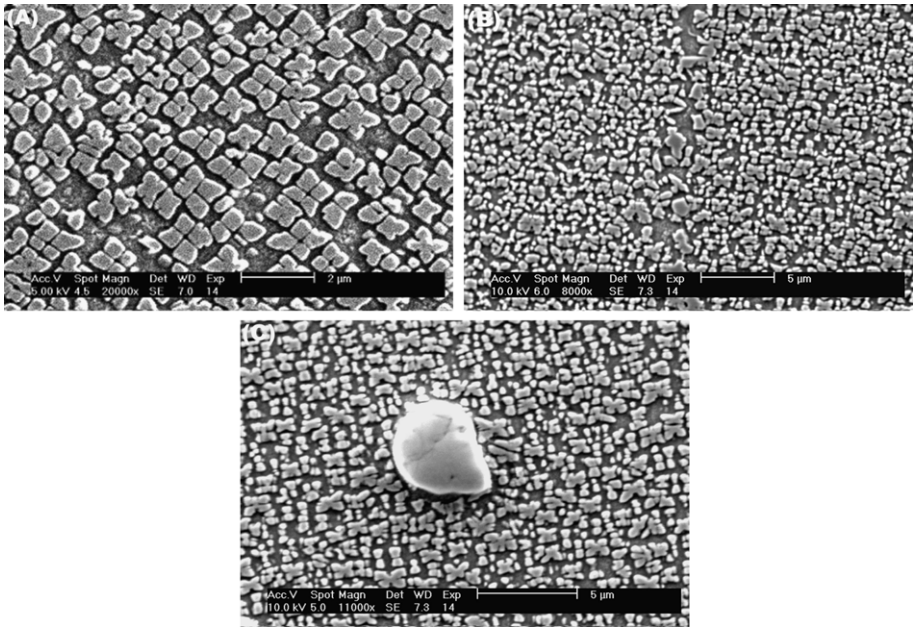

Fig. 9. SEM micrographs of damaged alloy after cycle F showing: (A) cuboidal γ′ precipitates within grain interiors; (B) grain boundary region; and (C) primary MC carbide.

SEM. Moreover, comparison of the grain boundary regions and MC carbides in the microstructure after cycle E (Fig. 8(b) and (c)) with those of the damaged alloy (Fig. 3(b) and (c)) implies that partial dissolution of grain boundary films and elimination of the transition zone around MC carbides have happened during the 1120 °C/2 h solution treatment.

It should be pointed out that the influence of cooling rate is more noticeable in the γ′ microstructure obtained after furnace cooling from solution treatment temperature. Fig. 9 shows the damaged microstructure after 1190 °C/4 h/FC solution treatment (cycle F). As can be seen in Fig. 9(a), the microstructure contains large cubes and octets of small cubes. In comparison with cycle D in which very fine γ′ precipitates formed during the air cooling after 1190 °C/4 h solution treatment (Fig. 7(a)), furnace cooling after the identical solution treatment (cycle F) produced relatively large unimodal–cuboidal cooling precipitates (Fig. 9(a)). Considering the data in Table 3, it is interesting to note that, among all cycles investigated in the current study, cycle F is the one which provided unique characteristics of cooling precipitates, *i.e.* the cooling precipitates with highest Feret diameter, volume fraction, and aspect ratio and lowest roundness (cubic morphology). The existence of such large cooling precipitates after cycle F is presumably due to the longer time available for diffusion of solute atoms and addition to the growing precipitates during the furnace cooling to room temperature [33]. Also, compared with the microstructures after cycles C and D (Figs. 6(a) and 7(a)), lower density of γ′ precipitates might be correlated with lower nucleation rate during furnace cooling.

The microstructure obtained after cycle G is shown in Fig. 10. As is evident, cycle G yielded a unimodal–cuboidal precipitate microstructure (Fig. 10(a)). Heat treatment cycle G is a

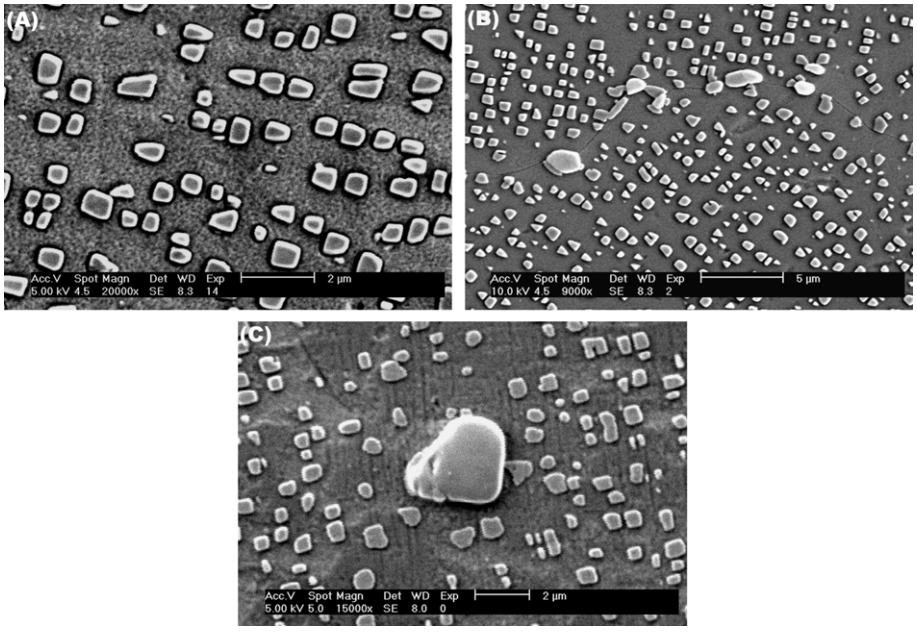

Fig. 10. SEM micrographs of damaged alloy after cycle G showing: (A) intragranular cuboidal γ′ precipitates; (B) grain boundary region; and (C) primary MC carbide.

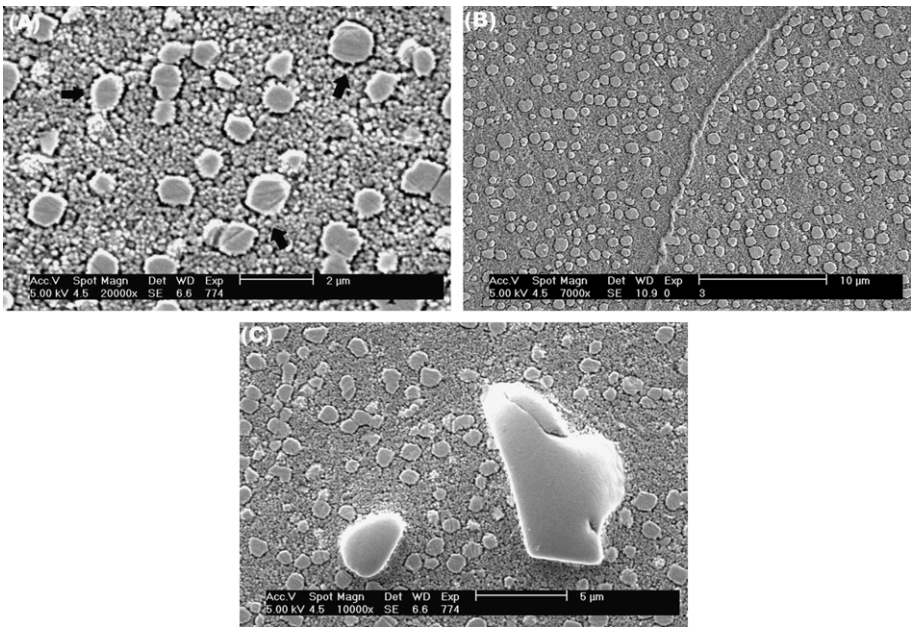

Fig. 11. Microstructure of damaged alloy after cycle H: (A) intragranular duplex size γ′ precipitates. Arrows indicate remnant precipitates; (B) continuous film on grain boundary area; and (C) primary MC carbide.

double solution treatment which involves a partial solution at 1120 °C/2 h/AC (cycle A) after a full solution treatment at 1190 °C/4 h/FC (cycle F). Considering the γ′ microstructures after cycles F and G (Figs. 9(a) and 10(a)), it can be found that the partial solution treatment resulted in partial dissolution of the coarse cuboidal γ′ particles which precipitated during the full solution treatment. Consequently, compared with the γ′ microstructure obtained after cycle F and consistent with the statistical data in Table 3, cycle G produced cuboidal γ′ precipitates with smaller size and lower volume fraction which are remains of the coarse cooling precipitates formed during the full solution treatment. In addition, as was the case for γ′ microstructure gained after heat treatment cycle A, due to high cooling rate during the air cooling, fine cooling precipitates were too small to be observed (within the limits of the SEM) in the vicinity of large cuboidal ones. Also, it is noteworthy that the microstructures obtained after cycles F and G showed grain boundary regions free from continuous films (Figs. 9(b) and 10(b)) and MC carbides without the transition zone in their perimeter (Figs. 9(c) and 10(c)). This might be attributed to the effect of 1190 °C/4 h solution treatment included in cycles F and G. That is, 1190 °C is high enough to eliminate the grain boundary films entirely and dissolve the transition zone around MC carbides.

3.3.2. *Effect of aging treatment*

In order to examine the influence of aging treatment on microstructure of the damaged alloy, heat treatment cycles H to J were conducted. Aging treatments were performed at 845 °C/24 h/AC condition after different solution treatments. The

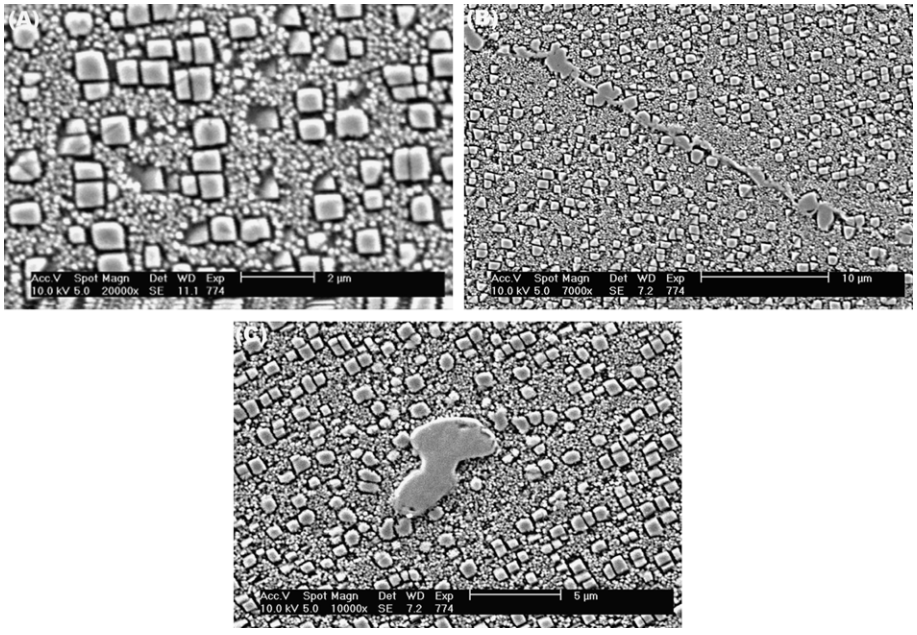

Fig. 12. SEM micrographs of damaged alloy after cycle I showing: (A) bimodal γ′ precipitates within grains; (B) grain boundary region; and (C) primary MC carbide.

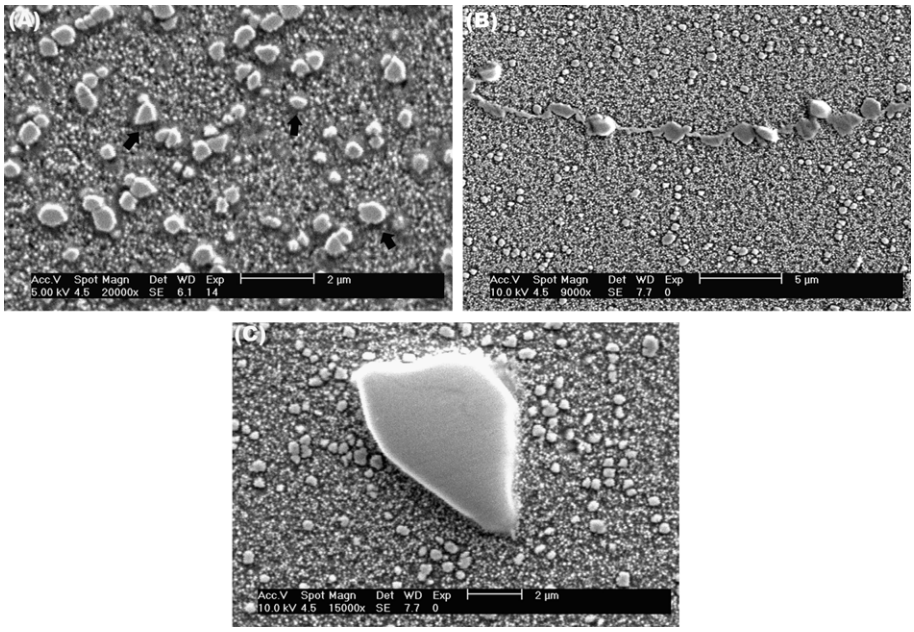

Fig. 13. Microstructure of damaged alloy after cycle J: (A) duplex size γ′ precipitates within grain interiors. Arrows indicate remnant precipitates; (B) grain boundary region; and (C) primary MC carbide.

γ′ microstructure obtained after heat treatment cycle H is shown in Fig. 11(a). Cycle H is, indeed, the standard heat treatment cycle for IN738LC alloy. It consists of 1120 °C/2 h/AC solution treatment (cycle A) and subsequent aging treatment. As can be observed in Fig. 11(a), cycle H produced a duplex-size precipitate microstructure. Considering the SEM micrographs from the microstructures after cycles A and H (Figs. 4(a) and 11(a)), it is obvious that a large number of fine secondary γ′ precipitates formed in the space between the coarse remnant ones during the aging treatment. The values of roundness and aspect ratio measured for γ′ precipitates (Table 3) indicate nearly spheroidal morphology for secondary precipitates. Furthermore, comparing the Feret diameters for remnant precipitates after cycles A and H, it can be deduced that some growth of remnant precipitates has happened during the aging. It is to be noted that the same effect of aging treatment was observed after cycle I. In cycle I, the damaged alloy was initially solution treated according to cycle G and aged subsequently. Comparison of the micrographs in Figs. 10(a) and 12(a) reveals that the aging treatment resulted in the formation of fine spherical secondary γ′ precipitates and some growth of cuboidal primary ones which formed after 1190 °C/4 h/FC + 1120 °C/2 h/AC solution treatment (cycle G). Formation of fine secondary precipitates and somewhat growth of primary ones appear to be related to the solute absorption from the supersaturated matrix during the aging.

It should be pointed out that, with respect to the MC carbides and grain boundary regions, the microstructures gained after cycles A and H (Figs. 4 and 11) are comparable. In both cases, due to the solution treatment at 1120 °C/2 h/AC, partially dissolved continuous films were remained on grain boundary regions and no evidence of transition zone can be observed around MC carbides. However, considering such features in the damaged microstructure after cycles G and I, it can be seen that, contrary to the grain boundary regions in the microstructure after cycle G (Fig. 10(b)), the grain boundaries were covered with irregularly shaped precipitates after aging treatment (Fig. 12(b)).

Heat treatment cycle J was carried out to investigate the effect of aging treatment on the microstructure obtained after 1160 °C/2 h/AC solution treatment (cycle B). The micrographs from the damaged alloy after cycle J are shown in Fig. 13. The values of roundness and aspect ratio for γ′ precipitates after cycles B and J (Table 3) reveal that there is no profound difference in morphology of γ′ precipitates before and after the aging treatment. In addition, no considerable changes can be observed in the MC carbides and intergranular regions (Fig. 13(b) and (c)). However, as seen in Table 3, the Feret diameters measured for γ′ precipitates in the microstructures before and after the aging treatment imply that little growth of γ′ precipitates has occurred during the aging. Such growth of γ′ precipitates during the aging treatment is likely due to particle coarsening *via* solute ejection from the matrix solid solution and addition to the growing precipitates.

The results of the present investigation show that the standard heat treatment for IN738LC alloy (cycle H) was not able to fully restore the damaged microstructure to the original state. However, among all heat treatment cycles investigated in the current study, cycle I is the only one that was successful in restoring the microstructure. The full solution treatment stage in cycle I led to dissolution of nearly all coarsened γ′ precipitates, continuous grain boundary films, and transition zone around MC carbides and following furnace cooling, partial solution, and aging treatments developed a new bimodal γ′ microstructure, containing cuboidal primary and spheroidal secondary γ′ precipitates. Moreover, grain boundaries without continuous films and MC carbides free from surrounding transition zone were observed after cycle I.

4. Conclusion

Conventionally cast IN738LC superalloy was initially damaged by interrupted creep test at 926 °C and stress level of 170 MPa for 200 h. The damaged alloy was then subjected to rejuvenation heat treatment cycles at different conditions to restore the degraded microstructure. The evolution of microstructural features during different stages of heat treatment cycles was studied. Based on the findings of this study, the conclusion could be summarized as the followings:

(1) Interrupted creep test gave rise to degradation of the virgin alloy. The microstructure deterioration is evidenced by coarsening and change in morphology and density of γ′ precipitates,

formation of continuous grain boundary films and development of transition zone around primary MC carbides.

(2) Solution treatment at γ' subsolvus temperatures resulted in partial dissolution of coarsened γ' precipitates and continuous grain boundary films and complete dissolution of transition zone around MC carbides in the creep damaged alloy. Also, the resultant microstructure after solution treatment consists of remnant and cooling γ' precipitates.

(3) Solution treatment at higher temperature resulted in smaller size and lower volume fraction of remnant precipitates, higher content of cooling precipitates and further dissolution of grain boundary films and yielded MC carbides free from surrounding transition zone.

(4) Although high temperature solution treatment (1190 °C/4 h) led to nearly complete dissolution of coarsened γ' precipitates, grain boundary films, and transition zone around MC carbides, it was not able to dissolve MC carbides.

(5) Slower cooling rates after solution treatment gave larger size of both remnant and cooling precipitates.

(6) Aging treatment led to the formation of new fine secondary precipitates and growth of the existing remnant and cooling precipitates which were obtained after the solution stage.

(7) Double solution treatment at 1190 °C/4 h/FC (furnace cooling) + 1120 °C/2 h/AC (air cooling) followed by aging at 845 °C/24 h/AC produced a new microstructure analogus with that of the virgin alloy.

References

[1] C.T. Sims, N.S. Stoloff, W.C. Hagel, Superalloys II, John Wiley & Sons, Inc., 1987.
[2] M.J. Donachie, S.J. Donachie, Superalloys: A Technical Guide, 2nd ed., ASM International, 2002.
[3] A.K. Jena, M.C. Chaturvedi, J. Mater. Sci. 19 (1984) 3121–3139.
[4] R.A. Stevens, P.E.J. Flewitt, J. Mater. Sci. 13 (1978) 367–376.
[5] R.A. Stevens, P.E.J. Flewitt, Mater. Sci. Eng. 37 (1979) 237–247.
[6] M. Durrand-Charre, The Microstructure of Superalloys, Gordon and Breach Science Publishers, Amsterdam, The Netherlands, 1997.
[7] H.M. Tawancy, N.M. Abbas, A.I. Al-Mana, T.N. Rhys-Jones, J. Mater. Sci. 29 (1994) 2445–2458.
[8] H. Xuebing, K. Yan, Z. Huihua, Z. Yun, H. Zhuangqi, Mater. Lett. 36 (1998) 210–213.
[9] E. Lvova, J. Mater. Eng. Perform. 16 (2007) 254–264.
[10] H.M. Tawancy, L. Al-Hdhrami, Eng Fail. Anal. 16 (2009) 810–815.
[11] P.W. Davies, J.P. Dennison, H.E. Evans, J. Inst. Met. 94 (1966) 270–275.
[12] R.V. Hart, H. Gyter, J. Inst. Met. 96 (1968) 338–344.
[13] P.W. Davies, J.P. Dennison, D. Sidey, J. Inst. Met. 101 (1973) 153–161.
[14] J.P. Dennison, P.D. Holmes, B. Wilshire, Mater. Sci. Eng. 33 (1978) 35–47.
[15] R.A. Stevens, P.E.J. Flewitt, Acta Metall. 27 (1979) 67–77.
[16] T.M. Maccagno, A.K. Koul, J.P. Immarigeon, L. Cutler, R. Allem, Metall. Trans. 21 (1990) 3115–3125.
[17] R.B. Girdwood, R.W. Evans, Int. J. Press. Vessels Piping 66 (1996) 141–153.
[18] J.A. Daleo, K.A. Ellison, D.H. Boone, J. Eng. Gas Turb. Power 124 (2002) 571–579.
[19] M.T. Kim, S.Y. Chang, J.B. Won, Mater. Sci. Eng. 441 (2006) 126–134.
[20] P. Wangyao, V. Krongtong, N. Panich, N. Chuankrerkkul, G. Lothongkum, High Temp. Mater. Process. 26 (2007) 151–159.
[21] A.K. Koul, R. Castillo, Metall. Trans. 19 (1988) 2049–2066.
[22] R.A. Stevens, P.E.J. Flewitt, Mater. Sci. Eng. 50 (1981) 271–284.
[23] M. McLean, H.R. Tipler, in: M. Gell (Ed.), Proceedings of the Fifth International Symposium on Superalloys, Metals Society of AIME, 1984, pp. 73–82.
[24] A.K. Koul, J.P. Immarigeon, R. Castillo, P. Lowden, J. Liburdi, in: S. Reichman (Ed.), Superalloys 1988, The Metallurgical Society, Champion, PA, 1988, pp. 755–764.
[25] E. Lvova, D. Norsworthy, J. Mater. Eng. Perform. 10 (2001) 299–313.
[26] Alloy IN738, Technical Data, INCO, New York, NY, pp. 1–11.
[27] G. Lvov, V.I. Levit, M.J. Kaufman, Metall. Mater. Trans. 35 (2004) 1669–1679.
[28] G. Jianting, D. Ranucci, E. Picco, P.M. Strocchi, Metall. Trans. 14 (1983) 2329–2335.
[29] A. Baldan, J. Mater. Sci. 26 (1991) 3409–3421.
[30] E. Balikci, A. Raman, R.A. Mirshams, Metall. Mater. Trans. 28 (1997) 1993–2003.
[31] I. Roy, E. Balikci, S. Ibekwe, A. Raman, J. Mater. Sci. 40 (2005) 6207–6215.
[32] A.K. Dwarapureddy, E. Balikci, S. Ibekwe, J. Mater. Sci. 43 (2008) 1802–1810.
[33] N. El-Bagoury, M. Waly, A. Nofal, Mater. Sci. Eng. 487 (2008) 152–161.